Mon. Not. R. astr. Soc. (1987) **227**, 361–372

Herbig Haro objects in the vicinity of NGC 2023

D. F. Malin, K. Ogura* and J. R. Walsh *Anglo-Australian Observatory, PO Box 296, Epping NSW 2121, Australia*

Accepted 1987 February 20. Received 1987 February 19; in original form 1986 November 3

Summary. Two groups of Herbig Haro objects have been discovered in the vicinity of the reflection nebula NGC 2023 and the Horsehead nebula (Barnard 33). Prime focus photographs, objective prism and low-dispersion spectra, and high-resolution line profiles have been obtained for the HH objects and proper motions have been derived for the brighter knots. Low-dispersion spectra of two possible exciting stars for the HH objects have also been obtained. The HH group closer to NGC 2023 shows a spatial distribution and proper motions suggesting a nearby faint star with an IR excess and strong Hα emission as the probable exciting source. However, no strong candidate was found for the exciting star of the second group of HH objects which are situated near V615 Ori and the base of the Horsehead nebula.

1 Introduction

The distinctive Horsehead Nebula (also known as Barnard 33, Barnard 1913) is part of the dusty complex of emission and reflection nebulae which are found in the southern part of the dark cloud L1630 (Lynds 1962). The region also contains the curious emission/reflection nebula NGC 2024 (Balick 1976) and the emission nebula IC 434 (S277, Sharpless 1959) which is excited by σ Orionis and into which the Horsehead Nebula intrudes. The dark cloud also contains several embedded sources, including V615 Ori (Kukarkin *et al.* 1967; Mannino 1959) and the conspicuous reflection nebula NGC 2023. The whole complex is at a distance of about 450 pc.

NGC 2023 is illuminated by HD 37903, a B1.5V star (Sharpless 1952) and appears blue on colour photographs. The reddening [$E(B-V)=0.36$, Lee 1968] to HD 37903 is much larger than to σ Orionis [$E(B-V)=0.06$], confirming that the former star is partially embedded in the L1630 cloud. The U, B and V colour maps of NGC 2023 are consistent with reflection of the radiation of HD 37903 by dust, but at R and I there is extended red (continuum) emission (ERE) in excess of that expected by simple scattering (Witt, Schild & Kraiman 1984). In the near-IR the nebula displays the 3.3 μm unidentified emission feature and extended continuum emission characterized by a colour temperature ~1200 K (Sellgren, Werner & Dinerstein 1983); the ERE represents

*On sabbatical leave from Kokugakuin University, Tokyo, Japan. Visiting astronomer, Cerro Tololo Inter-American Observatory which is operated by AURA Inc. under contract to the US National Science Foundation.

the short-wavelength tail of this continuum. It has been suggested by Sellgren (1984) that this emission arises from heating of small (molecular sized) grains to ~2000 K following absorption of a UV photon. Strom *et al.* (1975) found a number of 2 μm sources, identified with faint stars in the vicinity of NGC 2023, and Sellgren (1983) showed that there was a real excess of sources with $K>10$ mag, particularly to the south of HD 37903. Five stars with IR excess in the $(J-H)$ versus $(H-K)$ diagram were identified as probable pre-main-sequence stars and two of these showed Hα emission. The region has recently been surveyed in CO by White (1986, private communication) and his map shows complex structure around HD 37903 and V615 Ori.

We report here the discovery of two groups of Herbig Haro (HH) objects in the southern part of L1630. One group occurs at the edge of NGC 2023 itself and the other to the south and west, close to V615 Ori. Filter photography, objective prism and low-dispersion grating spectroscopy, proper motion measurement and échelle spectroscopy have been obtained in order to study these HH objects and their relation to local star formation.

2 Observations

2.1 DIRECT PHOTOGRAPHY

Three direct plates of the 1° field containing NGC 2023, 2024, B33 and IC 434 were obtained at the $f/3.3$ prime focus of the Anglo–Australian Telescope (AAT) on 1984 February 2–3. The triplet corrector was employed, giving a scale of 15.3 arcsec mm^{-1}. A *B*-plate (GG385+IIa-O) of 25 min exposure, a *V*-plate (GG495+IIa-D) of 25 min exposure, and an *R*-plate (RG610+098−04) of 35 min exposure were obtained in 1.5 arcsec seeing. Since it was intended to produce a colour composite image from the three plates, the II-a plates were developed for 8 min in D19 to match the contrast of the 098−04 plate, which was developed for the standard 5 min.

2.2 OBJECTIVE PRISM SPECTROSCOPY

A deep objective prism plate in the red was obtained of the NGC 2023–4 and IC 434 region with the 61/91-cm Curtis Schmidt at Cerro Tololo Inter-American Observatory on 1985 March 24. A 6° objective prism giving a dispersion of 600 Å mm^{-1} at Hα was employed. An RG630 filter and hypersensitized III-aF emulsion gave a pass-band of 6300–6900 Å. The exposure time was 90 min in ~3 arcsec seeing, and no widening was applied.

2.3 LOW-DISPERSION SPECTROSCOPY

The group of bright HH knots south-west of NGC 2023 (NGC 2023 HH1, see below) was observed with the RGO 25-cm camera mounted at the $f/8$ Cassegrain focus of the AAT on 1986 August 17. The 242 arcsec long slit was orientated east–west and centred on the group of knots. The slit length also included the southern extremities of the NGC 2023 reflection nebula. On 1986 December 22 the two fainter knots close to NGC 2023 HH1 – NGC 2023 HH4 and 5 (see below) – were observed with the same telescope and with the spectrograph slit orientated at a position angle of 39°, thus recording the spectrum of both objects. V615 Ori and Sellgren's star C (2023/108 of Strom *et al.* 1975) were also observed on this night. The 250 B grating was used, to give a spectral coverage of 3500–7200 Å and the detector was the Image Photon Counting System (IPCS). The exposure times ranged from 500 s for V615 Ori to 1200 s for NGC 2023 HH4 and 5 and a slit width of 240 μm (1.6 arcsec) was used giving a spectral resolution of ~7 Å. The seeing at the time of observation was ~2–3 arcsec.

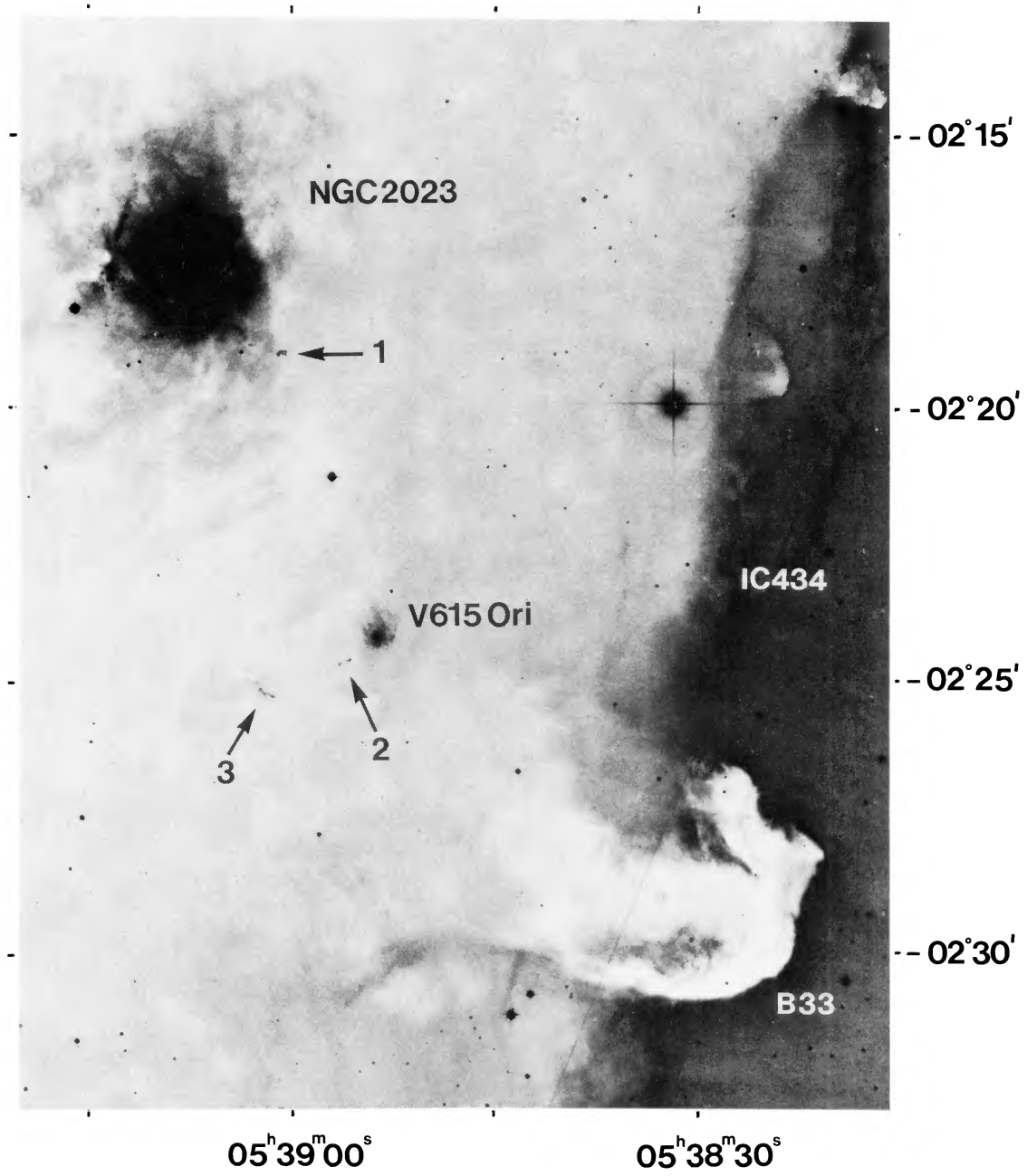

Plate 1. The NGC 2023 – Horsehead region. This print was derived from the AAT *R* plate and shows the location of the groups of Herbig Haro objects and the important features in the region. B1950 equinox coordinates are marked.

[*facing page* 362]

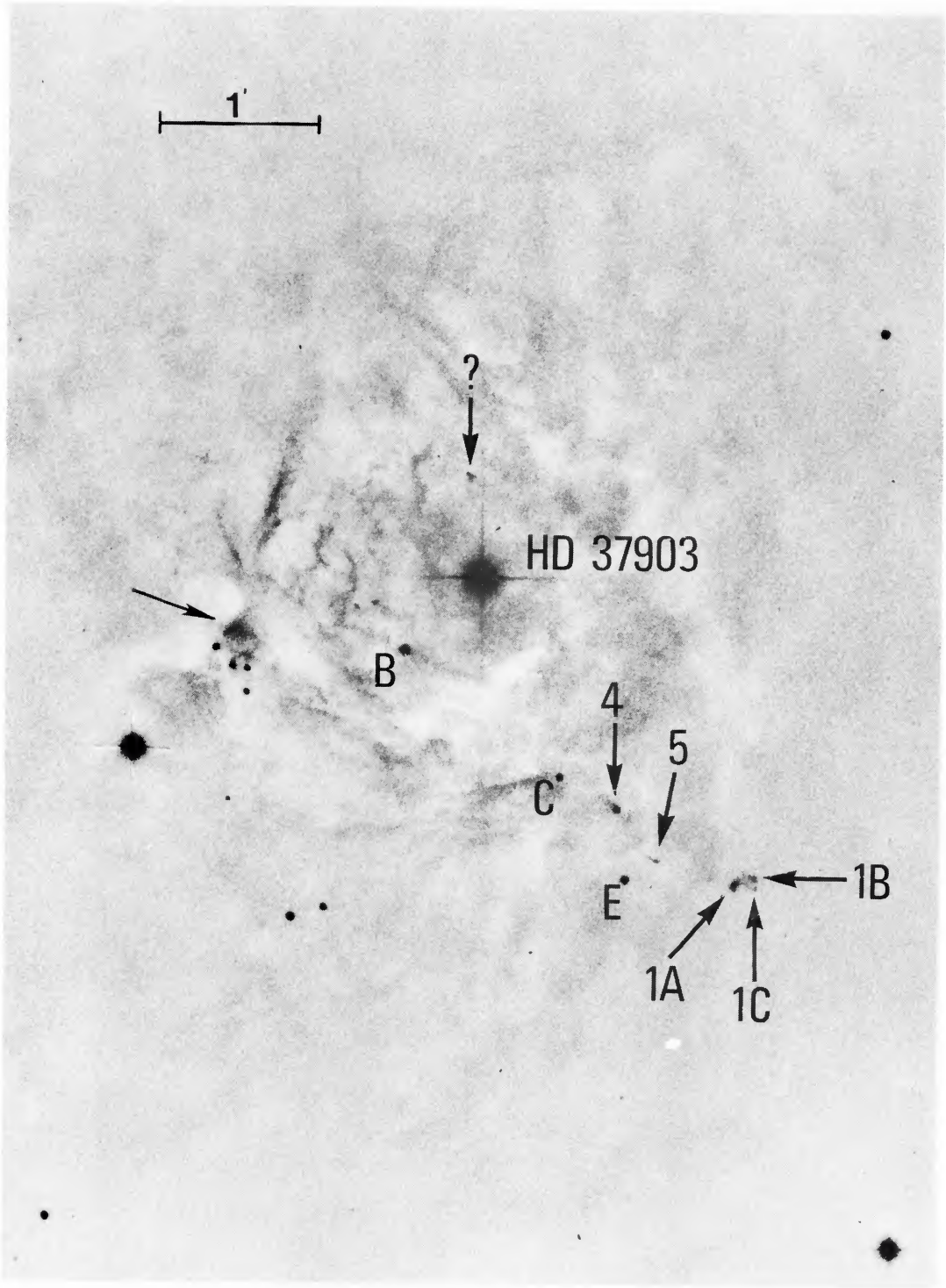

Plate 2. An unsharp masked print derived from the AAT *R* plate of the NGC 2023 region. HD 37903 is the bright star in the centre of the field and the positions of the confirmed HH objects and further candidates are indicated. The designations of the stars are from Sellgren (1983). North is at the top, east to the left.

2.4 ÉCHELLE SPECTROSCOPY

Two of the HH candidates (NGC 2023 HH1 and 3, see below) were observed with the Manchester échelle spectrograph (Meaburn *et al.* 1984) mounted at the $f/8$ Cassegrain focus of the AAT. A slit width of 150 μm (1.0 arcsec) was employed giving a measured spectral resolution of 12 km s^{-1} (FWHM). The 87th order of the échelle, including the Hα and [N II] 6548, 6583 Å lines, was isolated with an 80 Å wide interference filter centred at 6580 Å. The detector was again the IPCS and a useful slit length of 171 arsec was imaged on to 120 IPCS pixels (1.42 arcsec per pixel). The slit was centred on the HH candidates and was orientated east–west. Two exposures of 1800 s were obtained in seeing of 1.5 arcsec on 1984 November 3.

3 Results

3.1 DIRECT PHOTOGRAPHY

When positive copies of the *B*, *V* and *R* plates were combined additively into a three-colour picture (Malin 1980), three groups of red, non-stellar objects were found in the dark cloud region adjacent to NGC 2023. On the basis of their colour and non-stellar appearance they were considered to be Herbig Haro objects. Plate 1 is a high contrast print derived from the *R* plate of the NGC 2023 and B33 region with 1950 equinox coordinates. The objects are designated as NGC 2023 HH1–3 and are indicated on the photograph. NGC 2023 HH1 consists of a brighter eastern knot, which we have designated A, and two fainter knots B, to the north and west of A and knot C, due west of A. NGC 2023 HH2 consists of two bright knots designated as A and B with A west of B, whilst NGC 2023 HH3 is more complex and consists of at least three knots and filamentary structures, the brightest knot, A, being at the western end of the chain, with knot B roughly central and C at the eastern end. Table 1 lists the 1950 equinox, 1984.09 epoch coordinates of the HH knots, determined relative to six SAO stars on the plate. An unsharp masked (Malin 1978) print of the red plate showing the high spatial frequency information in NGC 2023 is shown in Plate 2; HD 37903 is the bright star in the centre of the field. Two further red knots, which are also HH candidates, are apparent on this print and are arrowed on Plate 2 as NGC 2023 HH4 and 5; neither is visible on the *B*- or *V*-plates down to the plate limit. The coordinate of NGC 2023 HH4, which was measured by the offsets from HD 37903 on the print, has a lower accuracy ($\mp$1 arcsec) since it could not be directly measured on the AAT plate because it was hidden in the dense image of the bright reflection nebula. Another red non-stellar knot is also apparent 39 arcsec north and 5 arcsec east of HD 37903 and is indicated by a question mark on Plate 2; it is considered as another HH candidate.

3.2 PROPER MOTION DETERMINATION

It is evident that many observatories have obtained excellent (prime focus) plates of the Horsehead region but we were unable to locate any of them to measure proper motions of the newly discovered HH objects. The only suitable plate available to us was a glass copy of the Palomar Sky Survey red plate (E435) taken on the coarse-grained 103a-E emulsion in 1951. With the AAT plate this provided a 33 yr baseline, which is adequate to obtain at least crude proper motions, despite the rather low plate scale and resolution of the Palomar plate. A high-contrast contact copy of the Palomar red plate was made on which HH objects 1, 2 and 3 were clearly visible. [The objects are also well seen on the SERC 1.2-m Schmidt *R*-band plate (R5437) taken with 098–04 emulsion in 1979.] All measurements were made on the Anglo–Australian Observatory PDS and each set of plate measurements was repeated with the plate rotated through 90°; the mean coordinates from both sets of measurements were adopted. The positions of 16 faint stars in

Table 1. Coordinates of Herbig Haro objects and candidates.

Object	RA			Dec		
	h	m	s	°	'	''
NGC2023 HH1A	05	39	00.86	-02	18	52.2
HH1B	05	39	00.37	-02	18	49.8
HH1C	05	39	00.35	-02	18	54.6
HH2A	05	38	55.58	-02	24	30.0
HH2B	05	38	56.33	-02	24	34.8
HH3A	05	39	01.31	-02	25	11.0
HH3B	05	39	01.90	-02	25	07.8
HH3C	05	39	02.21	-02	25	02.7
HH4	05	39	03.9	-02	18	24
HH5	05	39	02.85	-02	18	43.6

Equinox B1950.0; epoch 1984.09.

a 20 arcmin field which includes NGC 2023 and B33 were measured relative to 14 SAO stars on both E435 and R5437. Those which had unusual proper motions were then omitted and the remaining (10) stars were assumed to have the local motion of the region and were used as the set of reference stars against which the positions of the HH objects were measured on the Palomar and AAT plates. The positions of the HH objects on the AAT and Palomar plates were compared and the deduced proper motions in arcsec per century are listed in Table 3 for those HH knots which could be distinguished on both plates. In some cases the low plate scale and brighter limiting magnitude of the Palomar plate only allowed a mean position for two faint knots to be defined (e.g. NGC 2023 HH1BC). The total motion of the knots, the position angle of their motion and the deduced tangential velocity (assuming a distance of 450 pc) are listed in Table 2. Fig. 1(a) and (b) show the direction of motion of the individual knots in 500 yr for NGC 2023 HH1A, BC and HH2A, B and HH3A, B. The estimated error on the total motions is ~1.5 arcsec per century based on the rms errors in measurement of the secondary standards, but the actual error is almost certainly larger as a result of the problems arising in centroiding the faint diffuse objects.

3.3 OBJECTIVE PRISM SPECTROSCOPY

The objective prism plate shows double images of the unresolved Hα+[N II] (6548 and 6583 Å) lines and the [S II] (6716+6731 Å) line clearly for NGC 2023 HH1 and HH3. For HH1 the Hα+[N II] line has similar strength to [S II] whilst for NGC 2023 HH3 the [S II] line is the stronger. These elevated ratios of [S II] to Hα+[N II] confirm the HH nature of the spectra of these objects. NGC 2023 HH4 probably displays both emission lines and is almost certainly an HH object, although there is considerable confusion from a faint star in this vicinity of NGC 2023 (see Plate 2). For NGC 2023 HH2 the emission lines are also weakly present. LkHα 287 is listed by Herbig & Kuhi (1963) as an emission-line star and should be 16 arcsec north and 2.3 arcsec east of HD 37903. No star is, however, apparent at this position on Plate 2 but their identification chart shows that LkHα287 is Sellgren's star B (2023/101, Strom *et al.* 1975 and star No. 50 in the catalogue of stars with Hα emission of Haro & Moreno 1953). There is no trace of Hα emission from this star on the objective prism plate and Hα emission was not recorded by Sellgren (1983) so the Hα emission of LkHα 287 has probably faded since the earlier search.

Table 2. Proper motions of NGC 2023 HH objects.

Object		$\mu\alpha$ (Arcsec century^{-1})	$\mu\delta$	Velocity (kms^{-1})	Pa of velocity (^{o})
NGC2023	HH1A	-1.96	-0.84	58	247
	HH1BC	-3.07	-5.94	143	207
	HH2A	-5.50	+3.20	136	300
	HH2B	-7.69	+11.96	304	327
	HH3A	+2.93	+2.24	79	53
	HH3B	-2.61	-7.49	169	199

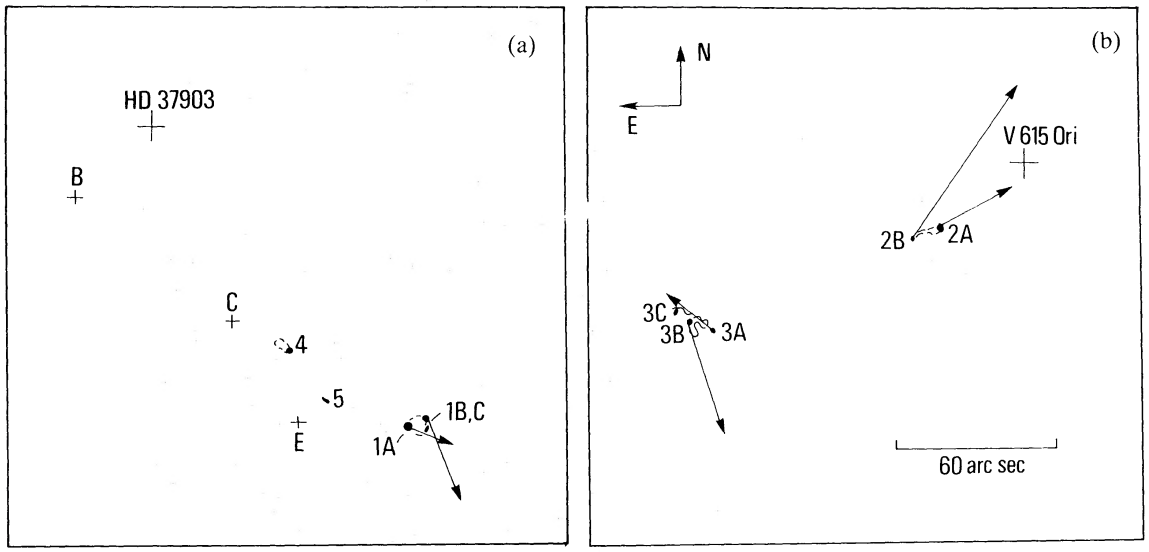

Figure 1. The direction and magnitude of the proper motions of the HH knots in 500 yr are shown against sketches of the regions. (a) Shows the motions of NGC 2023 HH1A and HH1BC and the position of HD 37903 and the other HH objects in the vicinity. (b) Shows the same for NGC 2023 HH2A and B and HH3A and B. Both figures have the same scale and orientation.

3.4 LOW-DISPERSION SPECTRA

3.4.1 HH objects

The spectra of NGC 2023 HH1, 4 and 5 and the spectrophotometric standard EG20 (Oke 1974) were wavelength-calibrated using exposures to a Cu–Ar comparison source. An atmospheric extinction correction was performed and the standard star spectrum was corrected for the effects of neutral density filters which prevented the count rate exceeding the non-linearity threshold of the IPCS. The long slit spectra were then flux calibrated. The emission-line strengths over NGC 2023 HH1, 4 and 5 were determined by subtracting the mean spectrum in adjacent channels along the slit and fitting Gaussians to the lines. For NGC 2023 HH1 the group of HH knots could be detected in seven channels along the slit and some asymmetry in the intensity distribution along the slit corresponding to HH1A and BC is apparent. However, the fairly low signal-to-noise ratio of the data precluded an analysis of the individual knots. For NGC 2023 HH4 the knot was detected in four channels along the slit and in two channels for HH5. The strong (predominantly blue) reflection nebula in the vicinity of NGC 2023 HH4 and 5 presents some problems for sky subtraction; the mean signal in at least twice as many channels as were occupied by the object was subtracted from the object spectrum. Table 3(a)–(c) lists the relative line fluxes and the errors arising from photon statistics and the continuum fit for NGC 2023 HH1, 4 and 5, respectively. Table 3(d) lists the line ratios for the surroundings (45 channels coadded along the slit to the west

Table 3. (a) Emission-line fluxes for NGC 2023 HH1.

REST WAVELENGTH (A)	LINE SPECIES	OBSERVED FLUX	ERROR	DEREDDENED FLUX	ERROR
3727	[O II]	143	21	358	52
4861	Hβ	100		100	
5158	[FeII]	59	15	45	12
5200	[N I]	64	16	48	12
6300	[O I]	485	60	177	22
6363	[O I]	120	30	42	10
6562	Hα	939	111	298	35
6583	[N II]	291	44	91	13
6717	[S II]	571	79	167	23
6731	[S II]	582	72	170	21

$F(H\beta) = 3.9 \times 10^{-15}$ Ergs cm^{-2} s^{-1}
C = 1.6
Av = 3.4
$N_e = 380$ cm^{-3}

Table 3. (b) Emission-line fluxes for NGC 2023 HH4.

REST WAVELENGTH (A)	LINE SPECIES	OBSERVED FLUX	ERROR	DEREDDENED FLUX	ERROR
3727	[O II]	124	12	296	30
4861	Hβ	100		100	
6300	[O I]	362	36	140	14
6363	[O I]	96	40	36	15
6562	Hα	878	78	298	26
6583	[N II]	396	41	134	14
6717	[S II]	552	55	175	17
6731	[S II]	594	60	187	19

$F(H\beta) = 1.8 \times 10^{-15}$ Ergs cm^{-2} s^{-1}
C = 1.5
Av = 3.3
$N_e = 460$ cm^{-3}

Table 3. (c) Emission-line fluxes for NGC 2023 HH5.

REST WAVELENGTH (A)	LINE SPECIES	OBSERVED FLUX	ERROR	DEREDDENED FLUX	ERROR
3727	[O II]	34	18	68	36
4861	Hβ	100		100	
6300	[O I]	198	52	95	25
6562	Hα	691	109	298	47
6583	[N II]	100	48	42	20
6717	[S II]	570	91	233	37
6731	[S II]	481	79	196	32

$F(H\beta) = 6.6 \times 10^{-16}$ Ergs cm^{-2} s^{-1}
C = 1.2
Av = 2.6
$N_e = 160$ cm^{-3}

of NGC 2023 HH1). The values of the logarithmic extinction, c, at Hβ were derived by comparing the observed Hα to Hβ line ratio with the case B recombination value for a temperature of 6000 K, and are listed in Table 3. The fifth column of Table 3 gives the reddening-corrected line ratios for the HH objects and the surroundings using the fit by Seaton (1979) to the mean Galactic reddening law with R=3.2. Since a separate sky exposure was not obtained, the line fluxes for the surroundings [Table 3(d)] are contaminated by night sky emission lines, which introduce an uncertainty of about ~10 per cent to the line fluxes. These surroundings show a characteristic low-excitation H II region spectrum ([O III] was not detected).

Table 3–*continued*

Table 3. (d) Emission-line fluxes for NGC 2023 surroundings.

REST WAVELENGTH (A)	LINE SPECIES	OBSERVED FLUX	ERROR	DEREDDENED FLUX	ERROR
3727	[O II]	152	5	181	6
4340	Hγ	37	2	41	2
4861	Hβ	100		100	
5200	[N I]	25	3	24	3
6563	Hα	373	14	301	11
6583	[N II]	122	8	98	6
6717	[SII]	55	5	43	4
6731	[SII]	45	4	36	3

$I(H\beta) = 3.5 \times 10^{-16}$ Ergs cm^{-2} s^{-1} $arcsec^{-2}$
C = 0.3
Av = 0.6
$N_e = 150$ cm^{-3}

Comparison of the relative line fluxes of NGC 2023 HH1 with the shock models of Shull & McKee (1978) suggests a shock velocity ~70–80 km s^{-1} from the [O II] and [N II] lines (with respect to Hβ) but ~50 km s^{-1} from [N I] and [S II]. However, the extinction correction may have been overestimated if the Hα/Hβ ratio of the shocked plasma differs significantly from the case B value (Shull & McKee 1978, list values of Hα/Hβ of 3.5–3.7 for shocks in the range 50 to 70 km s^{-1}). In addition there is evidence for anomalous extinction to HD 37903, characterized by a ratio of total to selective extinction, R, of 4.1 (Lee 1968; de Boer 1983; Massa, Savage & Fitzpatrick 1983), so that use of the Galactic reddening law with R=3.2 introduces a further source of uncertainty. For NGC 2023 HH4 the relative line fluxes suggest a shock velocity of ~100 km s^{-1} from [N II], [S II] and [O I] line strengths but less from the [O II] line; for NGC 2023 HH5 a value in the range 50 to 60 km s^{-1} is suggested from the [S II], [N II] and [O I] lines, but a low value from [O II]. The low shock velocity values derived from the [O II] line strength may be attributable to an unusual reddening law.

3.4.2 Stars

The spectra of V615 Ori and star C were reduced in the same way as the HH spectra and the data for V615 Ori were corrected for the effects of a neutral density filter. Both show broad Hα emission after the background emission had been subtracted and V615 Ori also shows emission in the core of the strong Hβ absorption line. The equivalent widths of Hα are 10 Å for V615 Ori and 49 Å for star C. V615 Ori is classified as of type G7 mainly on the basis of weak Ca I 4227 Å and Hδ absorption. The observed B–V colour is 2.0 compared with 0.8 for an unreddened G7 star. At a distance of 450 pc the absolute V-magnitude is 1.9, assuming a standard Galactic reddening law and a peak magnitude of 14 (Mannino 1959). The luminosity class of this star is thus III–IV and comparison of the dereddened spectrum with that of a G7III star from the Library of Stellar Spectra (Jacoby, Hunter & Christian 1984) shows that it is consistent with this spectral type. The weak Hα and Hβ emission may be evidence of an extended envelope, indicating mild T-Tauri properties, but no other lines are seen in emission; Ca II H and K are strongly in absorption. Star C shows much stronger Hα emission corresponding to T Tauri emission class 2–3 (Cohen & Kuhi 1979). Its noisy spectrum makes the classification difficult, but its spectral type is tentatively put at late G or early K on the basis of weak Na I and Mg I absorption. Its continuum shape, colours and extinction of ~3 mag are consistent with this spectral type. The V-magnitude of 17.69 given by Witt *et al.* (1984) indicates that this star is a dwarf.

3.5 RADIAL VELOCITY STRUCTURE

The long-slit échelle data were wavelength calibrated by a Cu–Ar comparison lamp spectrum and rebinned into constant wavelength increments. The slit across NGC 2023 HH1 showed peaks corresponding to HH1A and HH1BC. Fig. 2(a) shows the Hα emission-line profile over the whole of HH1ABC formed by coadding nine channels (~13 arcsec) along the slit. Across NGC 2023 HH3, knots A and B were not spatially resolved, but knot B has the stronger emission and Fig. 2(b) shows the Hα emission-line profile of NGC 2023 HH3AB (six channels coadded). The surroundings also show Hα and [N II] emission lines, presumably from the faint emission which is visible even in the darkest parts of L1630 on very deep photographs. Fig. 2(c) shows the mean Hα emission-line profile from the surroundings of NGC 2023 HH3. The mean emission in the surroundings was subtracted from the summed emission over the HH knots and the resulting line profiles were fitted by the minimum number of Gaussians required to simulate the observed profile; the residuals on the observed minus fitted profile being greater than or equal to the photon noise on the observed profile. The results of the fits in terms of heliocentric radial velocity, FWHM and relative flux in each fitted Gaussian are listed in Table 4. The photon noise on the observed profile, together with the mean deviation of the background continuum fit and the residuals on the fit are used to estimate the errors on the radial velocity and FWHM, and are also listed in Table 4 (columns 3 and 5). Only the fits on the Hα line are given. Fits to the [N II] 6583 Å line produced similar results but the errors are larger since the line has only about one third of the signal of Hα. The relative response of the spectrograph across the single order (i.e. blaze profile) was calibrated by an exposure to a tungsten-halogen lamp and was used to correct the [N II] strength to allow the total [N II]/Hα line ratio of each knot and the surroundings to be calculated. The resultant values for NGC 2023 HH1 and the surroundings were about 10 per cent higher than from the low-dispersion data, probably through uncertainty in the correction for blaze response. Therefore the [N II]/Hα ratio values presented in Table 4 have been scaled by the value for the surroundings from Table 3(d).

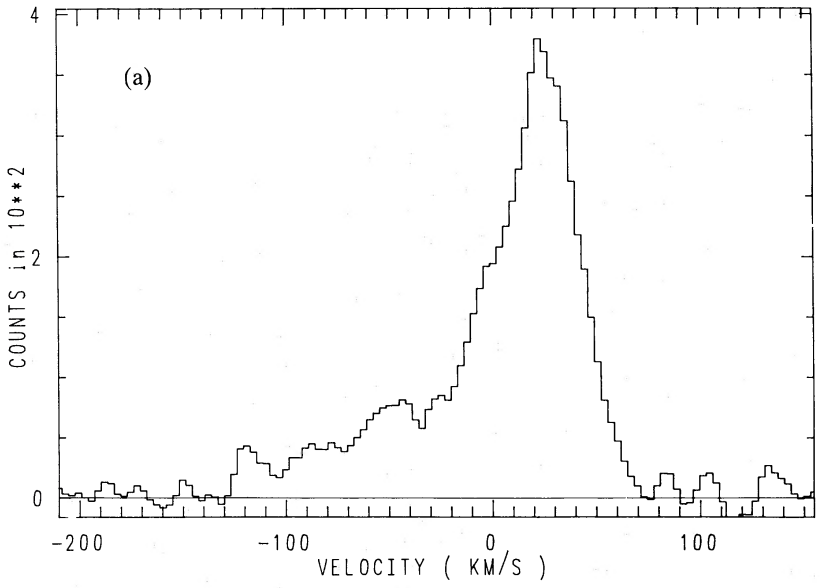

Figure 2. The Hα profiles of NGC 2023 HH1 and HH3, which display high negative velocity wings, are shown in (a) and (b), respectively. The profiles are those observed and the background emission has not been subtracted. (c) Shows the mean Hα profile from the surroundings (per pixel). Heliocentric radial velocity is plotted.

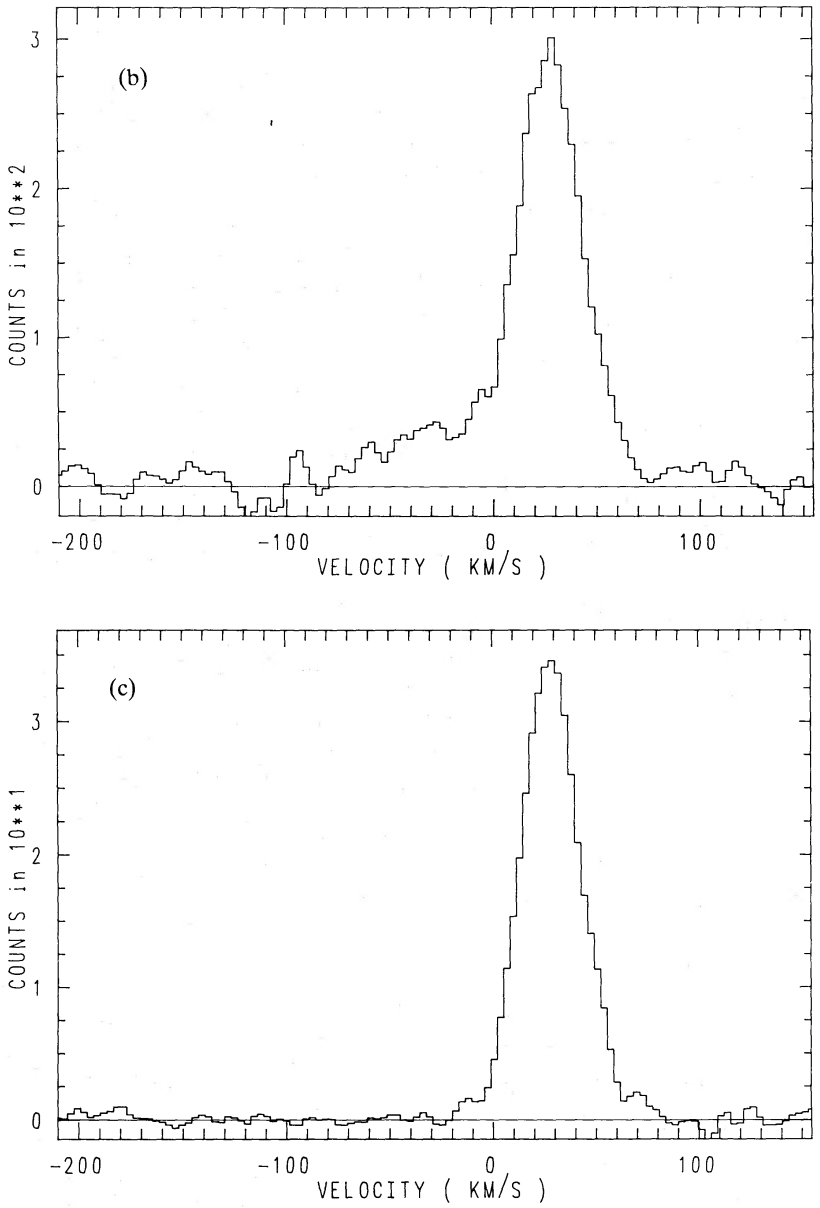

Figure 2–*continued*

Table 4. Radial velocity structure of the NGC 2023 HH emission-line profiles.

Object	Heliocentric Radial Velocity (kms^{-1})	Error (kms^{-1})	FWHM (kms^{-1})	Error (kms^{-1})	Line Flux (countsxA)	Total [NII]/Hα
NGC2023 HH1A	-100.6	22.3	64.2	10.0	51.7	
	-50.1	9.2	37.9	9.8	56.1	0.40
	-3.8	6.3	39.9	12.0	90.3	
NGC2023 HH1BC	-7.5	16.7	47.0	32.6	50.1	0.45
NGC2023 HH3AB	-30.3	21.0	56.1	14.0	48.6	
	+26.6	7.5	43.0	14.5	91.2	0.55
Surroundings						
Hα	+22.3	0.8	31.1	1.4	-	
[NII]	+23.0	1.1	24.1	2.7	-	0.44

4 Discussion

The two groups of Herbig Haro objects in the south of L1630, represent two and possibly three centres of low-mass star formation. The first group is that associated with NGC 2023 HH1, 4 and 5 (Table 1); their proximity and linear spatial distribution strongly suggest a close association. Such chains of HH objects are quite common – namely HH46–47 (Graham & Elias 1983; Meaburn & Dyson 1987), HH32 (Hartigan, Mundt & Stocke 1986) – and the present group shows similarities to the HH7–11 chain in the NGC 1333 region. On the basis of the morphology and direction of the proper motion vectors of NGC 2023 HH1, the exciting star is expected to be to the north-east. Three stars can be considered as candidates: HD 37903, Sellgren star B (2023/101, Strom *et al.* 1975) and Sellgren star C (2023/108, Strom *et al.* 1975; No. 49 in Haro & Moreno 1953). HD 37903 is of too early a spectral type (B1.5) to be the obvious exciting star of an HH object since its wind would be of too high velocity and too highly ionized to produce a low-excitation shock as inferred for HH objects. Sellgren's star B does not appear to be in the earlier pre-main sequence stage since it shows no IR excess (Sellgren 1983), but on the basis of its time varying Hα emission, it is probably a young star. However star C has a high probability of being a very young star since it shows a near-IR excess, is of typical T Tauri type being of late spectral type and showing strong Hα emission. The extinction is not large, being of the same order as that of the HH objects, so the star cannot still be heavily embedded in parental material. In addition, it appears to be closest to the HH group and is at the apex of the HH chain in the projected direction of the proper motion vector of NGC 2023 HH1A. The HH spectra are typical of low-excitation objects as predicted for low-velocity shocks (50–100 km s^{-1}); if HD 37903 were the exciting star the HH spectra would be expected to be less like HH spectra associated with cool star winds than an ionized wind. It is concluded that C is probably the exciting star for NGC 2023 HH1, 4 and 5, although no 10 μm emission, which is typical of an emerging young star, has been detected (Harvey, Thronson & Gatley 1980).

Mannion (1986, private communication) has studied the polarization of NGC 2023 and found a small reflection nebula about star C. The polarization vectors of the filament emanating from this star (see Plate 2) are, however, consistent with HD 37903 being the illuminating star for this feature. The region around star C is also close to the peak of the far-IR emission (Emerson, Furniss & Jennings 1975; Harvey *et al.* 1980) and C II recombination-line emission (Knapp, Brown & Kuiper 1975; Pankonin & Walmsley 1976, 1978). There is also extended CO, OH, H_2CO, HCN (Tucker, Kutner & Thaddeus 1973; Milman 1975; Milman *et al.* 1975) emission in this region. However, these features are most probably related to HD 37903 since a pre-main-sequence star would not be expected to produce a large ionized region and the IR luminosity is that expected for a B1.5V star. However, the position of star C is within 50 arcsec of the position of an intermediate velocity outflow source (ΔV=13 km s^{-1}) observed by Bally & Lada (1983), which may be related to star C and the HH chain. Mapping in ^{12}CO by White (1986, private communication) shows possible evidence of a bipolar outflow source centred on this area although there is much confusing structure in the region. It is possible that NGC 2023 HH4 and 5 have formed within the blueshifted lobe of a wind cavity whilst NGC 2023 HH1 has formed closer to the extremity of this cavity; the blueshifted CO emission in the maps of White and the high negative radial velocity of NGC 2023 HH1 lend credence to this proposal. This picture could be confirmed most directly from radial velocity measurements of NGC 2023 HH4 and 5. It would be useful to search to the north-east of star C for possible HH objects in the counter jet or lobe (expected to be redshifted and therefore to suffer greater extinction). The area of nebulosity arrowed in Plate 2 is the only candidate visible on the AAT plates; however this is adjacent to a neutral intrusion visible on the *B* and *V* plates so is possibly an ionization front.

The second group of Herbig Haro objects, NGC 2023 HH2 and 3, do not form an obvious

association. The proper motions suggest a possible exciting source between them since both are roughly directed away from their mid-point, although NGC 2023 HH3 fits less well into this picture. The faintness and filamentary nature of NGC 2023 HH3 may have contributed to large errors for the proper motion measurement. The large proper motions of NGC 2023 HH2 indicate that V615 Ori is probably not the exciting star. The *IRAS* point source catalogue lists V615 Ori (05388−0224) but the bolometric luminosity ($\sim 20\,L_\odot$ for a distance of 450 pc) is uncertain since there is extended 60 and 100 μm emission in this region (the cirrus flag is set); from the absolute magnitude a luminosity of $\sim 21\,L_\odot$ is inferred for a G7IV star. The low luminosity of V615 Ori puts it in the class of low-mass stars but its *IRAS* colours are not indicative of an HH exciting star (Rowan-Robinson 1987). No other *IRAS* point sources are found in this region. However, it would be difficult to distinguish a source within 2 arcmin of V615 Ori given the *IRAS* beam size. It is suggested that there may be an exciting star between NGC 2023 HH2 and 3, and a search at near-IR wavelengths is highly desirable. The high negative radial velocity of NGC 2023 HH3 indicates a flow out of the molecular cloud. It would be useful to determine the radial velocity of NGC 2023 HH2. If it showed a positive radial velocity then it would be another example of HH objects in a bipolar outflow source. Alternatively NGC 2023 HH2 and 3 could be excited by two independent stars undergoing mass loss. The CO maps of White (1986, private communication) show complex structure in this region, so this possibility merits further attention.

The association of HH objects with reflection nebulae and early-type (main sequence) stars suggests a possible scenario for the emergence of low-mass stars in such regions. Disruption of the cloud by mass loss and radiation pressure of young OB stars (HD 37903 for NGC 2023; ζ Ori and other embedded sources for NGC 2024) allows the mass loss from low-mass stars to become apparent in the form of high negative velocity emission in ionized gas (HH objects) and in neutral gas (molecular outflows). The implication is that low-mass stars may not have sufficient mechanical output in their winds to disrupt large molecular clouds. This may be the case for NGC 2023 HH1, 4 and 5. NGC 2023 HH2 and 3, however, are situated close to the base of the Horsehead and may be related to the disruption of the cloud which has resulted in the formation of the Horsehead. (B33 is assumed to be a foreground cloud since red emission (namely Hα, [N II] and [S II]) is apparent over the whole of the L1630 dark cloud in this region with the exception of parts of the Horsehead itself. This red emission may arise from the outer extensions of IC 434 or possibly by reflection from IC 434 given a suitable geometry. It is also possible that the disruption of the clouds by higher mass stars (*cf.* Elmegreen & Lada 1977) could initiate low-mass star formation through compression of the cloud medium and propagation of shocks leading to density enhancements. Several other instances of HH objects in the vicinity of reflection nebulae in large molecular clouds can be cited to support this view as one possibility for emergence of HH objects, e.g. HH19–27 and NGC 2068, HH1–3 and NGC 1999 and HH4–18 and NGC 1333 (Herbig 1974).

Acknowledgments

We thank J. Meaburn for allowing us to use the excellent Manchester échelle to obtain the line profiles of NGC 2023 HH1 and 3. KO is grateful to CTIO for telescope time and support for the objective prism observations. We also thank G. Herbig for searching, unfortunately without success, the Lick and Crossley archives for earlier plates showing the HH objects. M. D. Mannion and G. J. White very kindly sent results in advance of publication which have added greatly to the interpretation.

References

Balick, B., 1976. *Astrophys. J.,* **208,** 75.
Bally, J. & Lada, C. J., 1983. *Astrophys. J.,* **265,** 824.
Barnard, E. E., 1913. *Publs Lick Obs.,* **11**.
Cohen, M. & Kuhi, L. V., 1979. *Astrophys. J. Suppl.,* **41,** 743.
de Boer, K., 1983. *Astr. Astrophys.,* **125,** 258.
Elmegreen, B. G. & Lada, C. J., 1977. *Astrophys. J.,* **214,** 725.
Emerson, J. P., Furniss, I. & Jennings, R. E., 1975. *Mon. Not. R. astr. Soc.,* **172,** 411.
Graham, J. A. & Elias, J. H., 1983. *Astrophys. J.,* **272,** 615.
Haro, G. & Moreno, A., 1953. *Bol. Tonantz.,* **7,** 11.
Hartigan, P., Mundt, R., & Stocke, J., 1986. *Astr. J.,* **91,** 1357.
Harvey, P. M., Thronson, H. A. & Gatley, I., 1980. *Astrophys. J.,* **235,** 894.
Herbig, G. H., 1974. *Lick Obs. Bull., No. 658.*
Herbig, G. H. & Kuhi, L. V., 1963. *Astrophys. J.,* **137,** 398.
Jacoby, G. H., Hunter, D. A. & Christian, C. A., 1984. *Astrophys. J. Suppl.,* **56,** 257.
Knapp, G. R., Brown, R. L. & Kuiper, T. B. H., 1975. *Astrophys. J.,* **196,** 167.
Kukarkin, B. V. *et al.*, 1967. *General Catalogue of Variable Stars,* 2nd edn, Moscow.
Lee, T. A., 1968. *Astrophys. J.,* **152,** 913.
Lynds, B. T., 1962. *Astrophys. J. Suppl.,* **7,** 7.
Malin, D. F., 1978. *Am. Astr. Soc. Photo. Bull.,* **16,** 10.
Malin, D. F., 1980. *Vistas Astr.,* **24,** 219.
Mannino, G., 1959. *Publs Obs. Astr. Univ. Bologna,* **7**(10), 1.
Massa, D., Savage, B. D. & Fitzpatrick, E. L., 1983. *Astrophys. J.,* **266,** 662.
Meaburn, J. & Dyson, J. E., 1987. *Mon. Not. R. astr. Soc.,* in press.
Meaburn, J., Blundell, B., Carling, R., Gregory, D. F., Keir, D. & Wynne, C. G., 1984. *Mon. Not R. astr. Soc.,* **210,** 463.
Milman, A. S., 1975. *Astrophys. J.,* **202,** 673.
Milamn, A. S., Knapp, G. R., Kerr, F. J., Knapp, S. L. & Wilson, W. J., 1975. *Astr. J.,* **80,** 93.
Oke, J. B., 1974. *Astrophys. J. Suppl.,* **27,** 21.
Pankonin, V. & Walmsley, C. M., 1976. *Astr. Astrophys.,* **48,** 341.
Pankonin, V. & Walmsley, C. M., 1978. *Astr. Astrophys.,* **67,** 129.
Rowan-Robinson, M., 1987. Crafoord Symp. Astrophysical Aspects of the Interstellar Medium and Star Formation, *Phys. Scripta,* in press.
Seaton, M. J., 1979. *Mon. Not. R. astr. Soc.,* **187,** 75P.
Sellgren, K., 1983. *Astr. J.,* **88,** 985.
Sellgren, K., 1984. *Astrophys. J.,* **277,** 623.
Sellgren, K., Werner, M. W. & Dinerstein, H. L., 1983. *Astrophys. J.,* **271,** L13.
Sharpless, S., 1952. *Astrophys. J.,* **116,** 251.
Sharpless, S., 1959. *Astrophys. J. Suppl.,* **4,** 257.
Shull, J. M. & McKee, C. F., 1978. *Astrophys. J.,* **227,** 131.
Strom, K. M., Strom, S. E., Carrasco, L. & Vrba, F. J., 1975. *Astrophys. J.,* **196,** 489.
Tucker, K. D., Kutner, M. C. & Thaddeus, P., 1973. *Astrophys. J.,* **186,** L13.
Witt, A., Schild, R. E. & Kraiman, J. B., 1984. *Astrophys. J.,* **281,** 708.